Solid State Nuclear Magnetic Resonance 133 (2024) 101959

Contents lists available at ScienceDirect

Solid State Nuclear Magnetic Resonance

journal homepage: www.elsevier.com/locate/ssnmr

# Cooperative β-sheet coassembly controls intermolecular orientation of amphiphilic peptide-polydiacetylene conjugates

Tarunya Rao Sudarshan [a,1], Sujeung Lim [b,1], Jeffrey Li [a], Alicia S. Robang [a], Leel Mazal Liberty [a], Herdeline Ann M. Ardoña [b,c,d,e,*], Anant K. Paravastu [a,f,**]

[a] School of Chemical and Biomolecular Engineering, Georgia Institute of Technology, Atlanta, GA, 30332, United States
[b] Department of Chemical and Biomolecular Engineering, Samueli School of Engineering, University of California, Irvine, CA, 92697, United States
[c] Department of Chemistry, School of Physical Sciences, University of California, Irvine, CA, 92697, United States
[d] Department of Biomedical Engineering, Samueli School of Engineering, University of California, Irvine, CA, 92697, United States
[e] Sue & Bill Gross Stem Cell Research Center, University of California, Irvine, CA, 92697, United States
[f] Parker H. Petit Institute for Bioengineering and Biosciences, Georgia Institute of Technology, Atlanta, GA, 30332, United States

ARTICLE INFO

Handling Editor: Prof D Bryce

ABSTRACT

In this work, we elucidated the structural organization of stimuli-responsive peptide-polydiacetylene (PDA) conjugates that can self-assemble as 1D nanostructures under neutral aqueous conditions. The amino acid sequences bear positively or negatively charged domains at the periphery of the peptide segments to promote solubility in water while also driving assembly of the individual and combined components into β-sheets. The photopolymerization of PDA, as well as the sensitivity of the resulting optical properties of the polymeric material to external stimuli, highly depends on the structural organization of the assembly of amphiphilic peptide-diacetylene units into 1D-nanostructures. Solid-state NMR measurements on $^{13}$C-labeled and $^{15}$N-labeled samples show that positively charged and negatively charged peptide amphiphiles are each capable of self-assembly, but self-assembly favors antiparallel β-sheet structure. When positively and negatively charged peptide amphiphiles interact in stoichiometric solutions, cooperative coassembly dominates over self-assembly, resulting in the desired parallel β-sheet structure with a concomitant increase in structural order. These results reveal that rational placement of oppositely charged residues can control β-strand organization in a peptide amphiphile coassembly, which would have implications on the adaptive properties of stimuli-responsive biomaterials such as the peptide-PDAs studied here.

## 1. Introduction

The mechanism of many polymeric materials exhibiting stimuli-responsive optical property transitions is often tightly linked with their structural organization and dynamic nature. Among various π-conjugated polymers, polydiacetylenes [1] (PDAs) are widely used as materials for biosensing due to their chromatic responsiveness to various stimuli such as temperature [2–6], pH [7–9], solvent [10,11] and mechanical stress [12,13]. The chromogenic properties derive from ultraviolet (UV)-induced polymerization of diacetylene (DA) groups into PDAs, and the resulting conformational states of the conjugated backbone chain upon exposure to the stimuli. Since the carboxylic acid-terminated alkyl-DA groups would not spontaneously organize into nanofibers or arrange themselves for polymerization on their own under neutral aqueous conditions, incorporating peptides can mediate the arrangements of the peptide-DA amphiphiles to meet the geometric requirements (~5 Å and 45°) for topochemical polymerization in biologically relevant environments to support self-assembly, as illustrated in Fig. 1 [14,15]. Based on previous reports on amphiphilic peptides [16] and other peptide-bearing polydiacetylenes [14,17–21], we expected self-assembly in 1D micellar assembly under aqueous conditions, where the peptides form the outer shell and the alkyl chains

* Corresponding author. Department of Chemical and Biomolecular Engineering, Samueli School of Engineering, University of California, Irvine, CA, 92697, United States.
** Corresponding author. School of Chemical and Biomolecular Engineering, Georgia Institute of Technology, Atlanta, GA, 30332, United States.
*E-mail addresses:* hardona@uci.edu (H.A.M. Ardoña), anant.paravastu@chbe.gatech.edu (A.K. Paravastu).
[1] These authors contributed equally to the manuscript.

https://doi.org/10.1016/j.ssnmr.2024.101959
Received 20 May 2024; Received in revised form 12 August 2024; Accepted 19 August 2024
Available online 22 August 2024

form the inner core. Consequently, an idealized structure could be designed with a shell of peptidic regions arranged as parallel β-sheets, which can drive the peptide-DA monomer units to point in a single direction, leading to efficient polymerization and desired optical properties (See Fig. 1). To promote its usage toward physiologically relevant, biological applications, we are searching for mild assembly conditions that can minimize the introduction of harsh parameters, such as extreme pH conditions.

In this work, we employed solid-state NMR to evaluate peptide-mediated structural organization of chromogenic polymer nanostructures. We investigated assemblies of the following peptide amphiphiles: a positively charged KKKGV-PDA ($K_3$GV-PDA), a negatively charged DDDGV-PDA ($D_3$GV-PDA), and a 1:1 equimolar mixture of both peptide amphiphiles ($K_3$GV-PDA/$D_3$GV-PDA) at neutral pH. K, D, G, and V are single-letter abbreviations for amino acids, which we list from the C- to the N-terminus of the polypeptide chain, following a convention established in previous publications to denote the connectivity of the polymeric segment on the N-terminus. The amino acid sequence design places charged segments on the C-terminus periphery, followed by a G residue as a spacer before the V residue at the N-terminus. The incorporation of V residue was due to its high propensity to form β-sheets as previously reported [22–25]. On the N-terminus, adjacent to V, 10, 12-pentacosadiynoic acid is appended as the DA-bearing non-polar end of the amphiphilic monomer. The peptides serve as templates to mediate the topochemical photopolymerization and enhance solubility under aqueous conditions. Our prior work revealed that all three PDA systems exhibit a thermochromic behavior (*i.e.,* color changes when exposed to temperature), demonstrated by UV–vis absorbance spectra for the solution phase [26]. Optical measurements on the three PDAs under study indicated similar color reversibility for the coassembly and KKKGV-PDA ($K_3$GV-PDA) while showing lower color reversibility for DDDGV-PDA ($D_3$GV-PDA) [26]. While β-strand secondary structure remained prominent for the coassembly and KKKGV-PDA, DDDGV-PDA showed negligible presence of β-strands [26]. Previous work has also demonstrated that our coassembly of the charged peptide-amphiphiles is not perfectly alternating nor two self-assemblies coexisting in solution [26]. It had been proposed that side-chain interactions within the coassembled PDA act as templating factors, thus reducing susceptibility to conformational hysteresis compared to self-assembled PDAs.

The differences in the degrees of thermochromism of the PDAs under study make us wonder about the dependence of the molecular arrangement of PDAs on structural nuances behind self-assemblies and coassembly of the templating peptides. Notably, structural outcomes of the supramolecular organization of two complementary peptides are influenced by the extent of heterotypic vs. homotypic interactions, yielding structures comprised of both components (*i.e., cooperative co-assemblies*) or only with similar molecules (*i.e., self-sorted structures*) [27–32]. The self-assembly of highly charged species is seldom expected, and any observed assembly typically occurs under more drastic conditions [33]. Such self-assembly could present itself in an antiparallel arrangement to minimize energy. In contrast, like a traditional copolymerization process, coassembly could present itself in an *alternating*, *block*, or *random* distribution of the components along the axis of aggregation [31]. While sequence engineering provides a handle over the intermolecular interactions, complementarity or orthogonality of the interactions between the same and partner peptides is key to the selectivity of the coassembly structure outcomes.

2D exchange $^{13}C$–$^{13}C$ dipolar correlation (DARR [34]) measurements on KKKGV-PDA, DDDGV-PDA, and an equimolar mixture of the two reveal an antiparallel arrangement in the single component peptide-PDAs and a parallel arrangement in the mixture. Due to the highly charged nature of the peptide amphiphiles, we anticipated an antiparallel arrangement in the single component PDAs. Intuitively, oppositely charged peptide amphiphiles were expected to coassemble in neutral conditions. We used $^{13}C$ and $^{15}N$ uniformly labeled $K_2$ and $V_5$ residues in KKKGV-PDA ($KK_2KGV_5$-PDA); $D_2$ and $G_4$ in DDDGV-PDA ($DD_2DG_4V$-PDA). Labeling enhances 1D NMR and enables the determination of molecular arrangements using 2D DARR [35]. This labeling strategy helped us confirm that the equimolar mixture of the charged peptide amphiphiles coassembles into a parallel assembly, which is the preferred design.

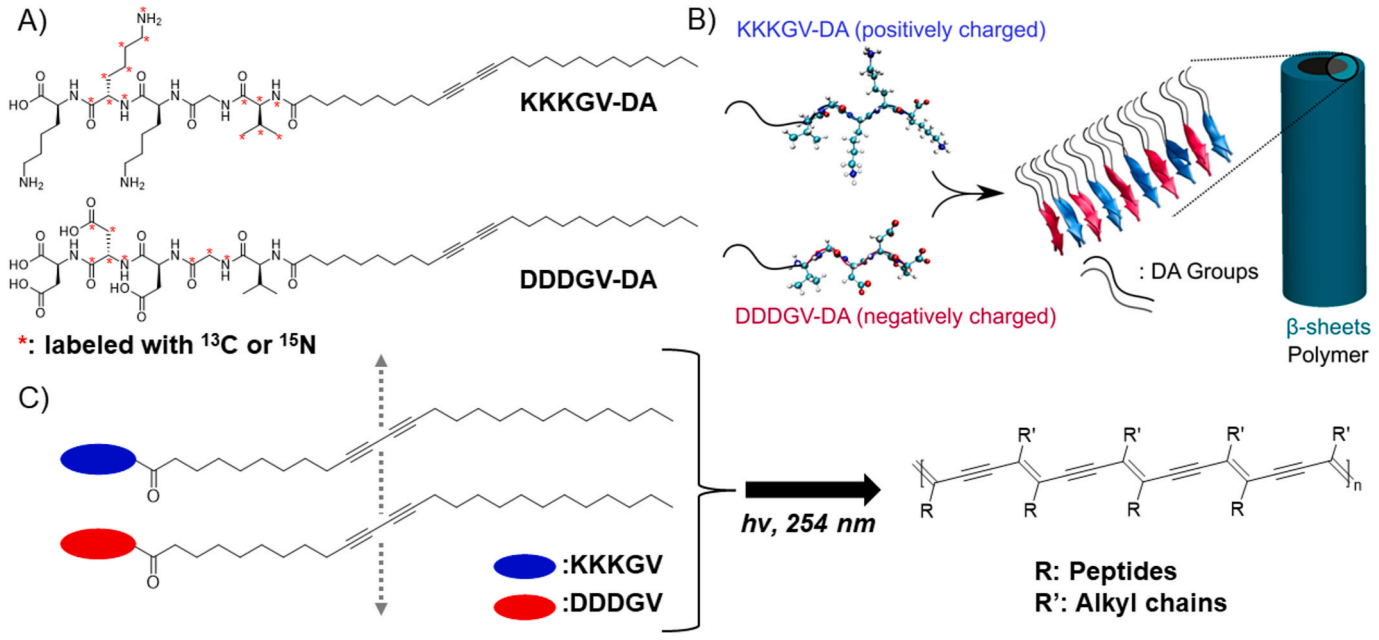


**Fig. 1.** A) Molecular structures of the peptide-DA amphiphiles ($K_3$GV-PCDA and $D_3$GV-PCDA) used in this study; *isotopically labeled sites. B) Schematic representation of an idealized parallel β-sheet assembly leading to 1D micellar peptide-PDA nanoassemblies. C) PDA polymerization scheme featuring two charged peptide-DA amphiphiles as the monomeric units.

## 2. Materials and methods

### 2.1. Sample preparation

*N*-methylpyrrolidinone (NMP), methanol, dichloromethane (DCM), dimethylformamide (DMF), ammonium hydroxide, potassium hydroxide (KOH), acetonitrile (ACN), *O*-(benzotriazole-1-yl)-*N,N,N′,N′*-tetramethyluronium hexafluorophosphate (HBTU), benzoatriazol-1-yl-oxy-tripyrrolidinophosphonium hexafluorophosphate (PyBOP), trifluoroacetic acid (TFA), triisopropylsilane (TIPS), *N*–*N*-diisopropylethylamine (DIPEA) were obtained from Oakwood Products, Inc. or Fisher Scientific. L-Aspartic acid-*N*-Fmoc, β-*O*-t-butyl ester ($^{13}C_4$, 99 %; $^{15}N$, 99 %), Glycine-*N*-Fmoc ($^{13}C_2$, 99 %; 15N, 99 %), L-Lysine-α-*N*-Fmoc, ε-*N*-t -Boc ($^{13}C_6$, 99 %; $^{15}N_2$, 99 %), L-Valine-*N*-Fmoc ($^{13}C_5$, 99 %; $^{15}N$, 99 %) were purchased from Cambridge Isotope Laboratories. The Wang resins and non-isotopically labeled Fmoc-protected amino acids were purchased from Advanced ChemTech. Formic acid and 10,12-pentacosadiynoic acid were purchased from Sigma-Aldrich. As explained in the introduction, KKKGV-Fmoc were designed to have labeled amino acids at positions 2 and 5, whereas DDDGV-Fmoc were designed to have labeled amino acids at positions 2 and 4. The isotope-labeled peptides ($KK_2KGV_5$ and $DD_2DG_4V$) were manually synthesized using the standard Fmoc solid-phase peptide synthesis (SPPS) technique following the same procedures as reported [26]. 10,12-PCDA coupling, and acid cleavage were done following the same procedure described previously [26]. $KK_2KGV_5$-DA and $DD_2DG_4V$-DA were purified using reverse-phase high-performance liquid chromatography (HPLC). The crude $KK_2KGV_5$-DA sample was dissolved in 0.1 % formic acid in Milli-Q water (pH 2–3), whereas $DD_2DG_4V$-DA crude sample was dissolved in 0.1 % ammonium formate in Milli-Q water (pH 8–9). An Agilent Infinity II Preparative HPLC system (column: Zorbax Eclipse XDB-C8, 21.2 × 250 mm) was used for the purification process. Electrospray Ionization Mass Spectrometry (ESI-MS) was done using a Waters Acquity ultra-performance liquid chromatography H-Class system to confirm the molecular weights of the samples. For the experiments listed below, peptide-polymer conjugates were prepared by using the amphiphilic peptide-diacetylenes $KK_2KGV_5$-DA and $DD_2DG_4V$-DA. First, 2.2 mM $KK_2KGV_5$-DA and 2.3 mM $DD_2DG_4V$-DA were prepared with pH 7 Milli-Q water. To prepare the individual component samples ($KK_2KGV_5$-DA and $DD_2DG_4V$-DA), each component was diluted with pH 7 Milli-Q water to have a final concentration of 1 mM. For the equimolar coassembly sample, we prepared each individual component ($KK_2KGV_5$-DA and $DD_2DG_4V$-DA) to have a concentration of 0.5 mM in the mixture, resulting in a combined monomer concentration of 1 mM. The samples were all exposed to a 254 nm UV light source (6 W) for 5 min to initiate the polymerization. The prepared samples were then centrifuged into 3.2 mm NMR rotors at 150,000g at 4 °C for 45 min on a Beckman Optima XPN-100 with a SW-41 Ti swinging-bucket rotor. The NMR rotors were held in a custom-made polycarbonate funnel widget fitted into 13.2 mL Ultra-Clear tubes.

### 2.2. NMR analysis

Solid-state NMR measurements were carried out on a 500 MHz Bruker spectrometer, with a 3.2 mm HCN MAS (magic angle spinning) probe and a 3.2 mm Bruker Low-E $^1H/^{13}C/^{15}N$ NMR probe. To calibrate, we measured the NMR signal of adamantane and verified its $^{13}C$ chemical shift relative to TMS which occurs at 38.38 ppm and 29.45 ppm [36]. 1D $^{13}C$ cross polarization magic angle spinning [37,38] (CPMAS) experiments were conducted at MAS rate of 10 kHz. DARR experiments were conducted at MAS rate of 10.5 kHz. Signals were averaged over 24 h of scanning for CPMAS. We employed DARR dipolar recoupling technique at a short mixing time of 20 ms to capture intra-residue off-diagonal peaks, also referred to as crosspeaks. A long mixing time of 500 ms was employed to observe additional crosspeaks corresponding to inter-residue proximities. Further details are discussed in the results section.

2D Gaussian peak fitting was used to identify crosspeak positions using custom code developed in Wolfram Mathematica 13. $^{13}C$ chemical shifts from the Biological Magnetic Resonance Bank [39] were used as initial guesses for Gaussian peak fitting. Spectral assignments were assigned to each labeled $^{13}C$ atom based on 2D exchange $^{13}C$–$^{13}C$ DARR measurements. These Gaussian peak fits enabled peak identification for $^1H$–$^{13}C$ CPMAS experiments and helped us to perform secondary shift analysis [40] in Table 2. Secondary shifts are calculated using the deviation of $^{13}C$–$^{13}C$ DARR spectral assignments from random coil chemical shifts. Negative CO and $C_\alpha$ Δδ values (<−0.5 ppm) and positive $C_\beta$ Δδ values (>0.5 ppm) are associated with β-strand secondary structure [40].

The root-mean-square deviation (RMSD) was calculated between the coassembly DARR spectrum and an addition spectrum of $DD_2DG_4V$-PDA and $KK_2KGV_5$-PDA to quantify the difference between the coassembly and self-assemblies. A sum spectrum of 50%–50% $DD_2DG_4V$-PDA and $KK_2KGV_5$-PDA mixture was produced by normalizing the average signal intensity of the self-assemblies from 0 to 200 ppm in both axes, then summing signals at corresponding points. The resulting spectrum was rescaled to match the signal intensity of the coassembly spectrum. The coassembly spectrum was linearly interpolated into the same dimensions and resolution as self-assembly spectra. No interpolation was necessary between $DD_2DG_4V$-PDA and $KK_2KGV_5$-PDA, as these spectra were taken using the same acquisition parameters. The RMSD was then calculated between the interpolated coassembly spectra and the sum spectra using the method reported by Qiang et al. [41]. with a signal amplitude threshold of 4 times the root-mean-square noise.

### 2.3. Molecular modeling

Ideal β-sheet models of the individual peptide monomers and a peptide coassembly were produced to probe atomic distances between labeled residues. All-atom molecular models were simulated using Nanoscale Molecular Dynamics (NAMD) [42,43] and visualized with Visual Molecular Dynamics [44] (VMD). PDB files of the DDDGV and KKKGV monomers were generated using the Molefacture plugin on VMD [44], with β-strand backbone torsion angles. A Wolfram Mathematica notebook was then used to organize the monomer strands into β-sheets, consisting of two layers of 10 strands each. The coassembly was constructed with a composition of 50% DDDGV and 50% KKKGV (5 strands of each peptide amphiphile). Following the simplest interpretation of DARR data, monomers of the peptide self-assemblies were placed in an anti-parallel arrangement, while the coassembly was placed in an in-register parallel arrangement. Artificial torsion angle, hydrogen bonding, and hydrogen bond angle constraints were calculated for each system using these conformations. NAMD [42,43] was then used to perform a sidechain optimization, simulate hydrogen bonding between β-strands, collapse β-sheet layers, and then perform a final energy minimization on the β-sheets.

## 3. Results

### 3.1. Description of samples

We studied three samples, which were assemblies of peptide amphiphiles isotopically labeled with uniform $^{13}C$ and $^{15}N$ at two amino acids. KKKGV-DA was isotopically labeled at $K_2$ and $V_5$, which we indicate with the notation $KK_2KGV_5$-DA (See Fig. 1A). DDDGV-DA was isotopically labeled at $D_2$ and $G_4$, which we indicate with the notation $DD_2DG_4V$-DA (See Fig. 1A). The first sample was an assembly formed in a solution of 1 mM $KK_2KGV_5$-DA. The second sample was an assembly formed in a solution of 1 mM $DD_2DG_4V$-DA. The third sample was an assembly formed in a solution of 0.5 mM $KK_2KGV_5$-DA and 0.5 mM $DD_2DG_4V$-DA. The solvent for all samples was Milli-Q water. All three samples were irradiated with a 254 nm UV light source (6 W) for 5 min

to polymerize spatially proximate DA groups and produce peptide-PDA (peptide/polydiacetylene) nanofibers. We refer to UV-irradiated, polymerized samples as "peptide-polymer conjugates." Our previous work on this system [26] reported the characterization of the resulting polymers from individual and mixed 1:1 peptide-DA components (non-isotopically labeled), wherein the experimentally determined majority molecular weights from gel permeation chromatography (GPC) are approximately within the same order of magnitude ($M_w \sim 10^8$ g/mol).

Table 1 describes the samples studied using NMR in this study. In the sections below, we will refer to each peptide-polymer conjugate as "Sample 1," "Sample 2," or "Sample 3" as needed.

### 3.2. $KK_2KGV_5$-PDA and $DD_2DG_4V$-PDA each self-assemble and exhibit evidence of antiparallel intermolecular arrangement

Fig. 2 shows $^{13}C$ CPMAS spectra of Sample 1($KK_2KGV_5$-PDA) and Sample 2 ($DD_2DG_4V$-PDA). Detection of this type of NMR signal indicates that each peptide amphiphile self-assembled since dissolved molecules do not pellet in an ultracentrifuge. For these samples, we observed $^{13}C$ NMR linewidths of ~2 ppm [45], indicating structural order that is higher than we would expect for unassembled peptides (>3 ppm [46,47]) and lower than what we would expect for a peptide crystal and the most ordered amyloids known (<1 ppm [47–50]). Although the inclusion of charged D or K amino acids could confer resistance to self-assembly, these molecules were clearly self-assembled. To facilitate interpretation, we annotated the $^{13}C$ NMR spectra in Fig. 2 with spectral assignments (correspondence between NMR peaks and $^{13}C$-labeled sites), determined from 2D DARR spectra presented next.

We performed 2D exchange $^{13}C$–$^{13}C$ DARR [34] experiments on self-assembled peptide/polymer conjugates. When 2D DARR measurements are conducted with 20 ms mixing time, they reveal off-diagonal peaks (crosspeaks) corresponding to $^{13}C$ atoms within the same residue. This pattern of crosspeaks facilitates spectral assignments, or determination of NMR peak corresponding to its respective $^{13}C$-labeled site. In contrast, longer mixing time (500 ms) experiments reveal crosspeaks between $^{13}C$ atoms on different amino acids [34]. We use the term "contact" to describe when 2D DARR indicates spatial proximity between isotopically labeled amino acids. In our interpretation of all-atom models, we refer to the distance between any pair of $^{13}C$-labeled residues as the shortest possible distance between any $^{13}C$ atom on one amino acid and any $^{13}C$ atom on the other amino acid, since this distance has the largest influence on our ability to detect contacts in 2D DARR spectra. We expect to detect 500 ms 2D DARR contacts between any pairs of $^{13}C$-labeled residues separated by 0.6 nm or less.

Fig. 3A and 3B show 2D exchange $^{13}C$–$^{13}C$ DARR spectra at 500 ms mixing time for self-assembled peptide/polymer conjugates. Spectral assignments for labeled $^{13}C$ sites on $K_2$ and $V_5$ are completed using partial peak assignments from the 20 ms mixing time DARR spectrum (Supplemental Fig. 1B). In Fig. 3B, these spectral assignments are shown with solid green and black lines respectively. Analysis of Fig. 3B shows inter-molecular crosspeaks (black-green circles) between labeled carbon sites on $K_2$ and $V_5$. The $K_2/V_5$ contact is consistent with an antiparallel arrangement of adjacent $KK_2KGV_5$ peptides, as modeled in Fig. 3D. Spectral assignments for labeled $^{13}C$ sites on $D_2$ and $G_4$ are completed using a 20 ms mixing time DARR experiment (Supplemental Fig. 1A). These spectral assignments are shown with solid blue and red lines respectively. This spectrum reveals crosspeaks (blue-red circles) between labeled carbons on $D_2$ and $G_4$. The observation of a $D_2/G_4$ contact aligns with the antiparallel arrangement of nearest-neighbor $DD_2DG_4V$ peptides, as depicted in Fig. 3C. However, in Fig. 3A, labeled carbons on $D_2$ and $G_4$ show more than one chemical shift marked with dashed blue lines and red lines. These dashed lines are denoted with lowercase residue notations respectively. These dashed lines also cause minor crosspeaks depicted by dashed blue-red circles. These minor crosspeaks indicate that $DD_2DG_4V$-PDA is structurally heterogeneous and may have at least two different structures, causing multiple chemical shifts for labeled carbons in $D_2$ and $G_4$. Interestingly, the secondary shifts of these minor structures are neither β-strand-like nor α-helical, suggesting a random coil structure. 2D DARR contacts also indicate some degree of antiparallel organization between adjacent molecules.

There is another important distinction that differentiates our interpretations of the 2D DARR spectra in Fig. 3A and 3B: while the $K_2/V_5$ contact observed for $KK_2KGV_5$-PDA likely corresponds to interactions between labeled $K_2$ and $V_5$ residues on neighboring molecules, the $D_2/G_4$ contact observed for $DD_2DG_4V$-PDA could result from intramolecular $^{13}C$–$^{13}C$ couplings. First, the $^{13}C$ NMR peak positions discussed subsequently are consistent with β-strand secondary structure for the $KK_2KGV_5$-PDA self-assembly but suggest departure from β-strand secondary structure for the $DD_2DG_4V$-PDA self-assembly. Even if a β-strand is assumed for $DD_2DG_4V$-PDA, the intramolecular distance between $D_2$ and $G_4$ is less than 0.6 nm (See Fig. 3C). Thus, while the $K_2/V_5$ contact is clear evidence of the antiparallel arrangement of adjacent molecules in the $KK_2KGV_5$-PDA self-assembly, the $D_2/G_4$ contact could be influenced by antiparallel inter-molecular arrangement in the $DD_2DG_4V$-PDA self-assembly or may be the result of intra-molecular couplings. The all-atom model of antiparallel pairs of β-strand explains the contacts observed in the 2D DARR spectra of $KK_2KGV_5$-PDA; alternatively, it is possible that the β-strands are antiparallel on neighboring strands within stacked β-sheets.

### 3.3. A 1:1 equimolar mixture of $KK_2KGV_5$-DA and $DD_2DG_4V$-DA formed a cooperative coassembly [31] with distinct molecular structure

Fig. 4A shows $^{13}C$ NMR spectrum obtained with $^{1}H$–$^{13}C$ CPMAS from the 1:1 equimolar mixture (0.5 mM $KK_2KGV_5$-DA and 0.5 mM $DD_2DG_4V$-DA) and the spectra obtained from the self-assembled peptide-polymer conjugates. The black spectrum is from Sample 3. The blue and red spectra are from Samples 1 and 2, which are also shown in Fig. 2. As with Samples 1 and 2, we used 2D DARR spectra discussed subsequently for the spectral assignments for Sample 3 in Fig. 4A. Gray vertical lines are drawn to highlight NMR peaks that are similar in frequency between the different samples. Aided by spectral assignment and the gray lines, we see that NMR peaks from labeled amino acids in Sample 3 appear at similar frequencies to peaks from the same labeled residues in Samples 1 or 2. Fig. 4B shows an overlay of the spectrum from Sample 3 and the sum of the spectra from Samples 1 and Sample 2 (purple spectrum). This figure illustrates that there was a change in some NMR peak positions for the 1:1 equimolar mixture, particularly for signals from $D_2$ and $G_4$ in $DD_2DG_4V$-PDA. Two prominent changes to the spectra are the large decrease in intensity from $G_4$ $C_\alpha$ in the 1:1 equimolar mixture spectrum and the changes in linewidths of $K_2$ $C_\alpha$, $D_2$ $C_\alpha$, $K_2$ $C_\delta$, $K_2$ $C_r$. Comparison of NMR signal intensity is qualitative in nature, as it is affected by structures and dynamics. In Fig. 4B, we test a simplistic assumption: If the solution of $KK_2KGV_5$-PDA and $DD_2DG_4V$-PDA exhibited only self-assembly and not heterotypic interactions, then this sample would exhibit a $^{13}C$ NMR spectrum that would match the normalized sum of the spectra from the signal-peptide samples. Not only would the structures of the self-assemblies match, but so would the dynamics. As demonstrated in Fig. 4B, the chemical shifts and linewidths exhibit significant variations between the self-assembly and co-assembly. Distinctive features observed in CPMAS NMR signals further support that the 1:1 equimolar mixture has a structure different from self-assembly. We can

**Table 1**
Description of samples.

| Sample | Initial Peptide Amphiphile Solution | Peptide-Polymer Conjugate Probed by NMR |
|---|---|---|
| 1 | 1 mM $KK_2KGV_5$-DA | $KK_2KGV_5$-PDA |
| 2 | 1 mM $DD_2DG_4V$-DA | $DD_2DG_4V$-PDA |
| 3 | 0.5 mM $KK_2KGV_5$-DA + 0.5 mM $DD_2DG_4V$-DA | $KK_2KGV_5$-PDA/$DD_2DG_4V$-PDA |

**Table 2**
Secondary chemical shift analysis for peptide/polymer conjugates under study. Each entry corresponds to the NMR chemical shift of the major peak, and the full width at half maximum linewidths of each peak are given in parenthesis.

| Peptide | Residue | CO | $C_\alpha$ | $C_\beta$ | $C_{\gamma(1)}$ | $C_{\gamma(2)}$ | $C_\delta$ | $C_\varepsilon$ |
|---|---|---|---|---|---|---|---|---|
| Sample 1 ($KK_2KGV_5$ -PDA) | $K_2$ | 172.4 (1.8) | 52.5 (1.2) | 34.5 (2.1) | 24 (1.3) | | 28.3 (2.7) | 40.7 (1.0) |
| | Δδ | −2.5 | −2.0 | 3.1 | | | | |
| | $V_5$ | 173.5 (2.0) | 57.8 (1.3) | 33.2 (1.9) | 20.2 (1.4) | 19.1 (0.9) | | |
| | Δδ | −1.1 | −2.7 | 2.0 | | | | |
| Sample 2 ($DD_2DG_4V$ –PDA) | $D_2$ | 172.5 (1.3) | 52.1 (1.5) | 34.4 (2.3) | 174.9 (1.4) | | | |
| | Δδ | −2.1 | −0.4 | −5.0 | | | | |
| | $G_4$ | 171.7 (1.1) | 46.2 (1.0) | | | | | |
| | Δδ | −1.5 | 2.8 | | | | | |
| Sample 3 (Coassembly) | $K_2$ | 172.7 (1.5) | 52.4 (1.3) | 34.1 (2.6) | 23.7 (1.6) | | 27.7 (1.8) | 40.3 (1.2) |
| | Δδ | −2.2 | −2.1 | 2.7 | | | | |
| | $V_5$ | 173.3 (1.6) | 58.2 (1.1) | 32.8 (1.6) | 19.6 (1.8) | 19.2 (0.8) | | |
| | Δδ | −1.3 | −2.3 | 1.6 | | | | |
| | $D_2$ | 172.6 (2.4) | 51.7 (1.9) | 40.2 (2.5) | 178.6 (2.1) | | | |
| | Δδ | −2.0 | −0.8 | 0.8 | | | | |
| | $G_4$ | 170.1 (2.0) | 42.7 (1.4) | | | | | |
| | Δδ | −3.1 | −0.7 | | | | | |

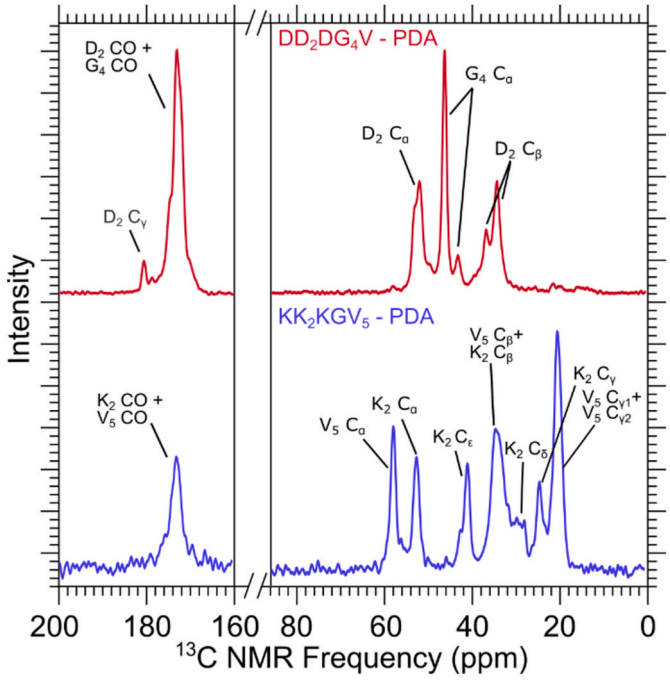


**Fig. 2.** 1D $^{13}C$ CPMAS results of self-assembled $KK_2KGV_5$-PDA (blue) and $DD_2DG_4V$-PDA respectively (red). Spectra were not processed with any window functions.

thus refer to the 1:1 equimolar mixture as a "coassembled peptide-polymer conjugate" or a "coassembly" in the manuscript owing to this distinct structure.

2D $^{13}C$–$^{13}C$ DARR measurements (500 ms) on Sample 3 revealed interactions between the two peptide amphiphiles (Fig. 5A). Spectral assignments for $K_2$, $D_2$, $G_4$, and $V_5$, determined using a 20 ms 2D DARR experiment (Supplemental Fig. 1C), are illustrated with green, blue, red, and black lines, respectively. Crosspeaks between distinct residues are labeled with bi-colored circles; we specifically observed crosspeaks between $G_4$ and $V_5$ (black/red) and between $K_2$ and $D_2$ (blue/green). Recalling that $D_2$ and $G_4$ were labeled on $DD_2DG_4V$-DA and $K_2$ and $V_5$ were labeled on $KK_2KGV_5$-DA, the contacts observed in Fig. 5A are between residues on different peptide sequences. We use the term "heterotypic" to identify contacts between amino acids on different peptide sequences, and the term "homotypic" to identify contacts between amino acids of the same peptide sequence. In fact, the 2D DARR spectrum from Sample 3 does not exhibit strong homotypic $K_2/V_5$ or $D_2/G_4$ contacts, which we observed in the self-assembled samples (Samples 1 and Sample 2). The DARR spectrum of $KK_2KGV_5$-PDA also exhibits stronger $K_2C_\alpha$- $V_5C_\alpha$ peaks which are barely above noise in the coassembly. $D_2/K_2$ contacts indicated by green-blue circles, present in aliphatic-aliphatic slice of Fig. 5A are indicative of a parallel arrangement between neighboring strands. Blue, red, and black dashed lines in Fig. 5A point to the existence of minor structures of $D_2$, $G_4$, and $V_5$ respectively, denoted in lowercase. Like the minor structure observed in the $DD_2DG_4V$-PDA assembly, the secondary shifts of $D_2$ and $G_4$ exhibit secondary shifts consistent with a random coil structure, while the $V_5$ minor structure still exhibits a secondary shift pattern consistent with a β-strand conformation. Surprisingly, Fig. 5A also shows an absence of $D_2/K_2$ contacts in the aliphatic/carbonyl region indicated by dashed blue-green circles. While these absent crosspeaks are ambiguous, ample $D_2/K_2$ contacts and $G_4/V_5$ suggest a dominant parallel arrangement between adjacent strands. Another unexplained ambiguity is the black dashed ellipse indicating signal growth of $K_2$ sidechains only in the long mixing DARR, but absent in the short mixing (See Supplemental Figs. 1C and 2C). Nevertheless, coassembly of the 1:1 equimolar mixture (Sample 3) produced a distinct structure from what was produced via self-assembly.

The observation of heterotypic 2D DARR contacts is evidence of cooperative coassembly of $DD_2DG_4V$-DA and $KK_2KGV_5$-DA. In a previous publication, we defined cooperative coassembly as a process mediated by heterotypic interactions of stoichiometric quantities of distinct peptides [31]. Fig. 5B shows a model coassembled β-sheet with a structure that is consistent with the 2D DARR spectrum in Fig. 5A. This model predicts distances of less than 0.6 nm between pairs of $D_2$ and $K_2$ residues as well as between pairs of $G_4$ and $V_5$ residues, consistent with the $D_2/K_2$ and $G_4/V_5$ contacts in Fig. 5A. While this model also predicts intramolecular distances of 0.6 nm between $D_2$ and $G_4$, we did not observe a $D_2/G_4$ contact in Fig. 5A. Noting that the inter-residue distance threshold for observing contacts in 2D $^{13}C$–$^{13}C$ DARR is not known precisely, the lack of $D_2/G_4$ contact in Fig. 5A suggests that the $D_2/G_4$ contact observed in Fig. 3A was either due to inter-molecular proximity or a molecular conformation that differed between the $DD_2DG_4V$-PDA self-assembly and the $DD_2DG_4V$-PDA/$K_2KKGV_5$-PDA coassembly. The β-strand conformation predicted in Fig. 5B corresponds to the largest possible intramolecular distance between $D_2$ and $G_4$. The all-atom model in Fig. 5B which shows perfect alternation between the oppositely charged peptide-amphiphiles is only a possible interpretation of the contacts detected from the DARR spectrum. Stacking between β-sheets can also result in similar contacts. Perhaps most importantly, the pattern of inter-residue contacts from Sample 3 indicates parallel, not

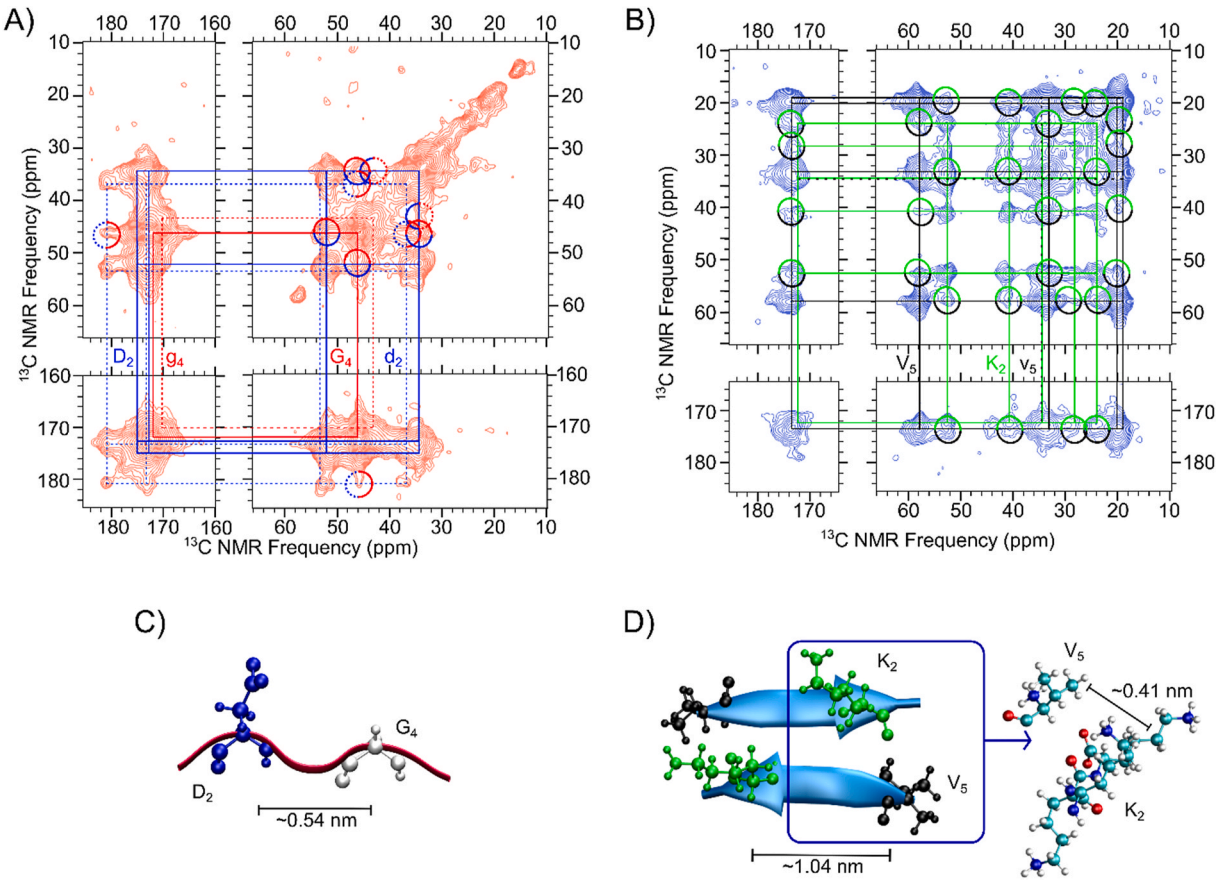


**Fig. 3.** A) 2D DARR results for assembled $DD_2DG_4V$-PDA. B) 2D DARR (500 ms mixing time) results for assembled $KK_2KGV_5$-PDA. Both 2D DARR spectra were processed in Bruker Topspin using exponential multiplication with a line broadening of 150 Hz. C) All-atom model of $DD_2DG_4V$ peptide strand showing intramolecular $D_2$ and $G_4$ proximity. D) All-atom model of an antiparallel $KK_2KGV_5$ β-sheet showing $K_2$ and $V_5$ proximity.

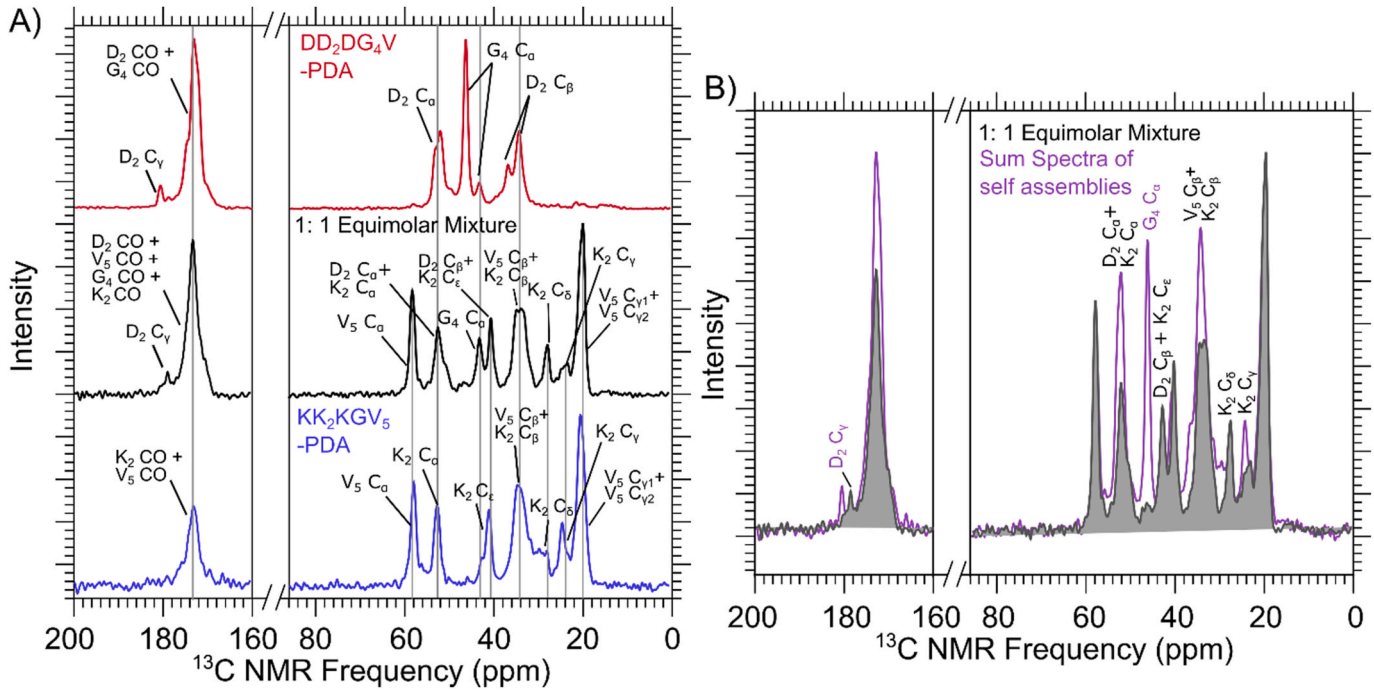


**Fig. 4.** A) 1D $^{13}$C CPMAS results of Sample 1 ($KK_2KGV_5$-PDA), Sample 2 ($DD_2DG_4V$-PDA) and a 1:1 equimolar mixture (Sample 3: $KK_2KGV_5$-PDA/$DD_2DG_4V$-PDA); Gray lines originating from the 1:1 equimolar mixture spectrum continuing to the self-assembly spectra highlights similarities between the self-assembly and 1:1 equimolar mixture. B) Added spectra of both self-assemblies (purple) compared to the 1:1 equimolar mixture spectrum. Only peaks that do not match the coassembly are highlighted, with purple colored text signifying presence only in the self-assembly spectra.

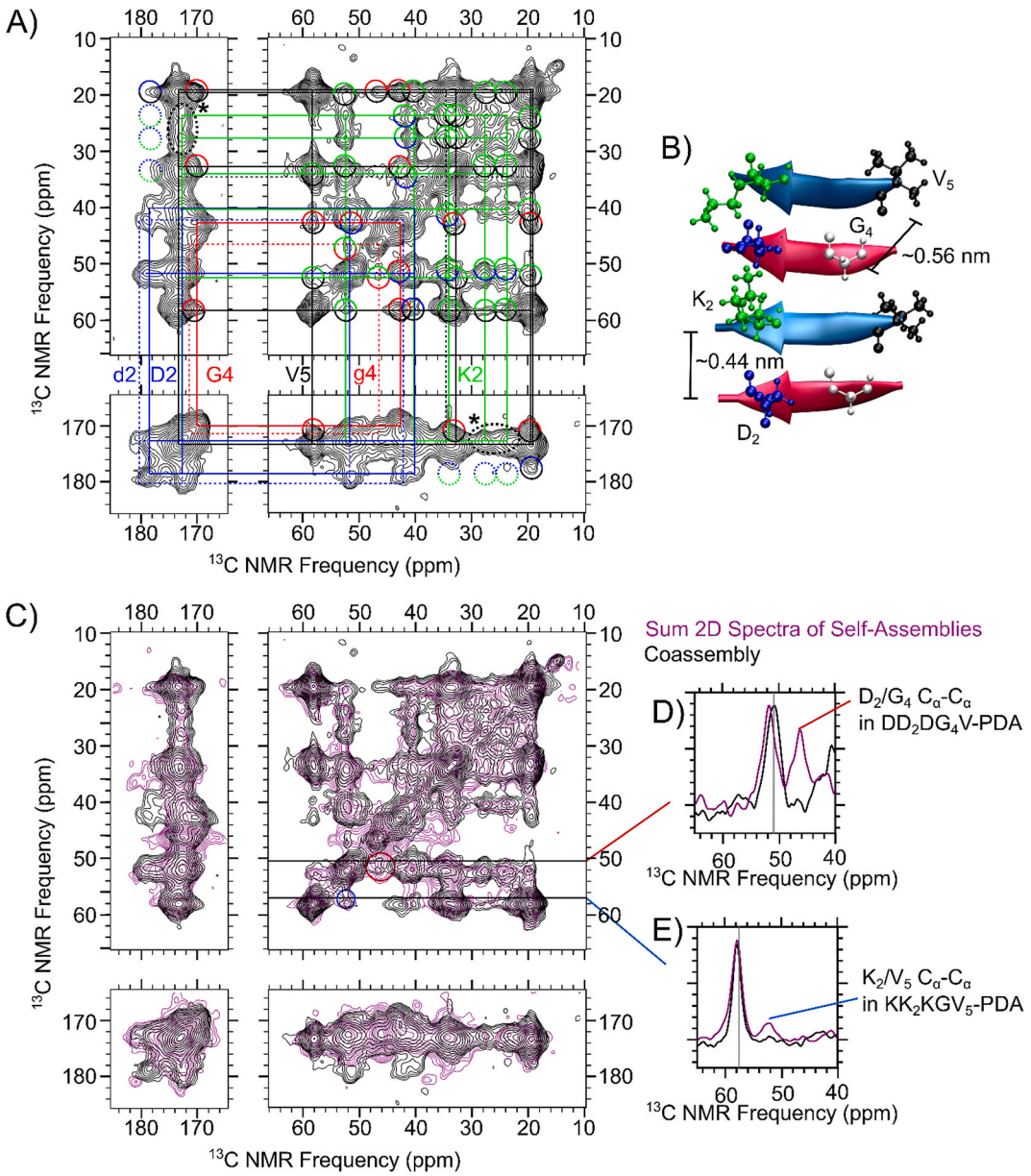


**Fig. 5.** A) 2D $^{13}$C–$^{13}$C DARR (500 ms) results for coassembly ($KK_2KGV_5$-PDA/$DD_2DG_4V$-PDA. Spectra were processed in Bruker Topspin using an EM window function with 150 Hz of line broadening. B) All atom model depicting a parallel coassembled β-sheet between $KK_2KGV_5$-PDA and $DD_2DG_4V$-PDA C) 2D DARR results for coassembly overlayed with sum 2D spectra of both self-assemblies (normalized). D) 1D NMR Slice at 50.5 ppm from Fig. 3A showing $D_2/G_4$ $C_\alpha$-$C_\alpha$ peak. E) 1D NMR Slice at 57.5 ppm from Fig. 3B showing $K_2/V_5$ $C_\alpha$-$C_\alpha$ peak.

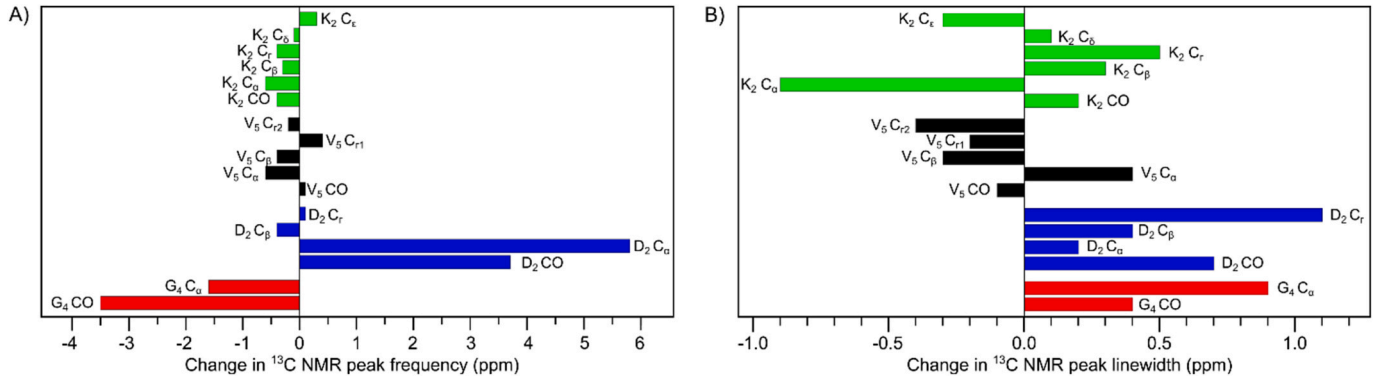


**Fig. 6.** A) Bar chart depicting change in $^{13}$C NMR peak frequency (ppm) for each labeled $^{13}$C atom. B) Bar chart depicting change in $^{13}$C NMR peak linewidth (ppm) for each labeled $^{13}$C atom. The term 'change' refers to a difference in the linewidth/frequency from the self-assembly to the coassembly.

antiparallel, organization of adjacent β-strands. This pattern supports the intended structure in the molecular design (see Fig. 1B).

Figs. 5B and 6, and Table 2 provide additional means of comparison between the coassembled Sample 3 and the self-assembled Samples 1 and 2. Fig. 5B is an overlay of the 2D $^{13}C$–$^{13}C$ DARR spectrum for Sample 3 (black contours) and the sum of the 2D $^{13}C$–$^{13}C$ DARR spectra from Samples 1 and 2 (purple contours). Fig. 5D and E exhibit slices from this spectrum, showing crosspeaks between $D_2$ $C_\alpha$ and $G_4$ $C_\alpha$ and between $K_2$ $C_\alpha$ and $V_5$ $C_\alpha$ are clearly observed for the self-assemblies but not for the coassembly. Following the method reported by Qiang et al. [41], we calculated a RMSD of 0.341 ppm between the aliphatic regions of black and purple spectra in Fig. 5A. Qiang et al. [41] suggested that RMSD values above 0.25 ppm indicate differences in structure, which is also evident from the lack of overlap in black and purple contours. In Fig. 6A, we use bar charts to show how $^{13}C$ NMR chemical shifts changed between the self-assembled and coassembled samples. The absolute frequencies of the peak positions are reported in Table 2. We observed the largest changes in NMR peak frequency for $^{13}C$-labeled sites in $D_2$ and $G_4$ within $DD_2DG_4V$-PDA. Consistently, secondary chemical shift analysis of $^{13}C$ NMR frequencies for backbone $^{13}C$ atoms (CO, $C_\alpha$, and $C_\beta$) indicates that the secondary structure for $DD_2DG_4V$-PDA in Sample 2 was not a β-strand but was a β-strand in Sample 3. Comparison of $^{13}C$ chemical shifts between Samples 1 and 3 indicates β-strand secondary structure for both $KK_2KGV_5$-PDA in both samples. Finally, Fig. 6B shows that we observed an increase in most NMR linewidths with coassembly when compared to the self-assembly indicating lower structural order.

## 4. Discussion

The results indicate that coassembly of $DD_2DG_4V$-DA and $KK_2KGV_5$-DA molecules successfully promoted parallel β-sheet structure. Although we also observed self-assembly in the single peptide-PDA samples, 2D $^{13}C$–$^{13}C$ NMR indicates contacts consistent with antiparallel molecular arrangements, *i.e.,* $D_2/G_4$ within $DD_2DG_4V$-PDA and $K_2/V_5$ within $KK_2KGV_5$-PDA (see Fig. 3A and B). In the sample produced by 1:1 equimolar mixture of $DD_2DG_4V$-DA and $KK_2KGV_5$-DA solutions, we observed significant changes to $^{13}C$ NMR peak positions, the reduction of NMR signals corresponding to homotypic contacts, and the emergence of heterotypic contacts consistent with parallel arrangements, *i.e.,* $D_2/K_2$ and $G_4/V_5$ (see Fig. 4A and B and Table 2). We interpret these results to indicate that cooperative coassembly of $DD_2DG_4V$-DA and $KK_2KGV_5$-DA occurred in the 1:1 equimolar mixture and that this process dominated self-assembly processes which could have occurred in the same solution. Consistently, $^{13}C$ secondary chemical shift analysis indicates β-strand secondary structure for $KK_2KGV_5$-PDA and the coassembly, but not $DD_2DG_4V$-PDA (see Table 2). These results are harmonious with results from our previous report [26], where we postulated that interactions between oppositely charged sidechains obtained via coassembly stabilize structures underlying thermochromic properties. Although previous optical measurements did not provide direct evidence that the oppositely charged D and K sidechains interact between nearest-neighbor peptide amphiphile molecules, the 2D DARR contacts do provide such evidence of interaction. Furthermore, the 2D DARR results are also consistent with our previously reported circular dichroism (CD) spectra [26]: DDDGV-PDA exhibited little β-strand secondary structure, while the KKKGV-PDA self-assembly and the coassembly exhibited typical β-strand signatures. To our knowledge, this system exhibits first-of-its-kind behavior: we are aware of no previously reported system of co-assembling peptides that also self-assemble under neutral, non-triggered aqueous conditions. Similarly, we are aware of no literature precedent for self-assembling peptides for which coassembly can drive the system to a distinct β-strand organization. In our previous studies of peptide co-assemblies, we observed that these systems tend to exhibit little control of β-strand organization. Thus, for coassembly, the placement of charged residues at the N-terminal ends of the peptides and the hydrophobic DA groups on the C-terminal ends of the peptides appears effective at producing parallel β-sheets.

Secondary shift analysis revealed that the coassembly produced a distinct structure not observed in either self-assembly. $DD_2DG_4V$-PDA showed a non-β-strand structure in the self-assembly but presented itself as β-strand in the coassembly. We suggest that the non-β-strand structure in the self-assembled structure of $DD_2DG_4V$-PDA may have contributed to the diminished color change reversibility we observed previously with temperature cycling. However, the NMR peak linewidths for labeled $^{13}C$ atoms in $D_2$, $G_4$, $K_2$, and $V_5$ in the self-assemblies are larger than the corresponding peaks in the coassembly (see Fig. 6B). Furthermore, we observed evidence of multisite occupancy (multiple NMR peaks for single labeled sites) in the 2D spectrum for $DD_2DG_4V$-PDA and the coassembly, which we did not observe for the same labeled sites for $KK_2KGV_5$-PDA. Since $KK_2KGV_5$-PDA has lower heterogeneity than $DD_2DG_4V$-PDA, it seems that is a level of disorder accompanies $DD_2DG_4V$-PDA and induces heterogeneity in the coassembly. Previous studies [51,52] have shown that coassemblies can have lower structural order than corresponding self-assemblies. In the current study, coassembly shows linewidths of 2–3 ppm which is lower structural order than most ordered amyloids with linewidth ~1 ppm [47–50].

While the present findings support the successful organization of peptide amphiphile molecules via coassembly, we raise questions about the relationship between molecular structure and optical properties. Firstly, our previous study [26] demonstrated absorbance spectra consistent with DA polymerization for DDDGV-PDA, KKKGV-PDA, and the coassembly. Thus, the antiparallel arrangement of KKKGV-PDA and the presence of relative disordered structures in DDDGV-PDA do not prevent UV light from polymerizing DA groups. It can be argued that stacking of antiparallel β-sheets makes it possible for DA groups to arrange sufficiently close for polymerization. Second, the heterotypic pattern of 2D DARR crosspeaks exhibited by the coassembly does not uniquely determine its structure. For example, our choice of isotopic labels made experiments sensitive to heterotypic parallel combinations of nearest-neighbor β-strands (via $D_2/K_2$ and $G_4/V_5$ contacts), or homotypic antiparallel combinations of nearest-neighbor β-strands (via $K_2/V_5$ contacts), but our experiments were not sensitive to homotypic parallel near-neighbor β-strands. Hence, the 2D DARR data do not necessarily indicate perfect alternation of KKKGV and DDDGV peptides within β-sheets. We suggested that homotypic nearest neighbors exist (*e.g.*, blocks of DDDGV or KKKGV) based on previous UV–vis absorbance spectra [26]. Thus, while coassembly clearly prevents complete self-sorting of KKKGV and DDDGV, it may not result in perfect alternation of KKKGV and DDDGV within β-sheets.

To summarize, the present results support the desired structure and highlight the effectiveness of solid-state NMR for evaluating molecular organization in peptide-PDA assemblies. However, the results also highlight significant challenges for the design of peptide amphiphile assemblies. Designing peptide assemblies is challenging even without the incorporation of functional groups such as DA. When groups such as DA are introduced, human intuition and available computational tools [53] may be less reliable. For instance, when CD curves indicate a non-β-strand secondary structure, as we observed for DDDGV-PDA, one may not have anticipated the observed self-assembly. This unexpected result could potentially be attributed to the hydrophobic nature of DA and was particularly influential on the assembly of short peptide sequences. Overall, our results support the importance of sequence design and consideration of complementary charges that influence the structural outcomes of self-sorted and coassembled structures. This work demonstrates the relevance of such concepts in peptide coassembly to these hybrid materials. In this case, the patterning of charged residues could favor heterotopic over homotypic interactions and parallel over antiparallel nearest-neighbor associations, which are otherwise challenging to control even in known sequences that form β-sheet structures.

## Author contributions

AKP and HAMA supervised the research. TRS, SL, AKP, ASR and HAMA designed the experiments. SL performed synthesis, purification, and characterization of the materials. SL prepared the samples used to study in this project. TRS conducted NMR experiments; TRS and JL analyzed NMR data. TRS, JL and LML modeled the samples presented in the images of this study. TRS, SL, JL, HAMA and AKP contributed to drafting the initial manuscript and revisions. All authors discussed the results and contributed to the final manuscript.

## Declaration of competing interest

The authors declare that they have no known competing financial interests or personal relationships that could have appeared to influence the work reported in this paper.

## Data availability

Data will be made available on request.

## Acknowledgements

This work was partially supported by the National Science Foundation (DMR-2239647 to H. A. M. A.). The authors acknowledge the use of instruments at the NMR Center at the Georgia Institute of Technology. This work was supported by the National Institute on Aging of the National Institutes of Health and the National Institute on Minority Health and Health Disparities (award number RF1AG073434-01A1). The content is solely the responsibility of the authors and does not necessarily represent the official views of the National Institutes of Health.

## Appendix A. Supplementary data

Supplementary data to this article can be found online at https://doi.org/10.1016/j.ssnmr.2024.101959.

## References

[1] J.T. Wen, J.M. Roper, H. Tsutsui, Polydiacetylene supramolecules: synthesis, characterization, and emerging applications, Ind. Eng. Chem. Res. 57 (28) (2018) 9037–9053, https://doi.org/10.1021/acs.iecr.8b00848.
[2] I.S. Park, H.J. Park, J.-M. Kim, A soluble, low-temperature thermochromic and chemically reactive polydiacetylene, ACS Appl. Mater. Interfaces 5 (17) (2013) 8805–8812, https://doi.org/10.1021/am402701n.
[3] N. Mergu, Y.-A. Son, Design and synthesis of polydiacetylenes, and their Low temperature irreversible thermochromic properties, Dyes Pigments 184 (2021) 108839, https://doi.org/10.1016/j.dyepig.2020.108839.
[4] X. Chen, J. Yoon, A thermally reversible temperature sensor based on polydiacetylene: synthesis and thermochromic properties, Dyes Pigments 89 (3) (2011) 194–198, https://doi.org/10.1016/j.dyepig.2009.12.015.
[5] S. Lee, J. Lee, H.N. Kim, M.H. Kim, J. Yoon, Thermally reversible polydiacetylenes derived from ethylene oxide-containing bisdiacetylenes, Sensor. Actuator. B Chem. 173 (2012) 419–425, https://doi.org/10.1016/j.snb.2012.07.031.
[6] S. Lee, J. Lee, M. Lee, Y.K. Cho, J. Baek, J. Kim, S. Park, M.H. Kim, R. Chang, J. Yoon, Construction and molecular understanding of an unprecedented, reversibly thermochromic bis-polydiacetylene, Adv. Funct. Mater. 24 (24) (2014) 3699–3705, https://doi.org/10.1002/adfm.201304147.
[7] F. Jannah, J.-M. Kim, PH-sensitive colorimetric polydiacetylene vesicles for urease sensing, Dyes Pigments 169 (2019) 15–21, https://doi.org/10.1016/j.dyepig.2019.04.072.
[8] W. Chen, S. Hazoor, R. Madigan, A.A. Adones, U.K. Chintapula, K.T. Nguyen, L. Tang, F.W. Foss, H. Dong, Alkaline-responsive polydiacetylene-peptide hydrogel for PH-sensing and on-demand antimicrobial release, Mater Today Adv 16 (2022) 100288, https://doi.org/10.1016/j.mtadv.2022.100288.
[9] M. Weston, R.P. Kuchel, M. Ciftci, C. Boyer, R. Chandrawati, A polydiacetylene-based colorimetric sensor as an active use-by date indicator for milk, J. Colloid Interface Sci. 572 (2020) 31–38, https://doi.org/10.1016/j.jcis.2020.03.040.
[10] S. Dolai, S.K. Bhunia, S.S. Beglaryan, S. Kolusheva, L. Zeiri, R. Jelinek, Colorimetric polydiacetylene–aerogel detector for volatile organic compounds (VOCs), ACS Appl. Mater. Interfaces 9 (3) (2017) 2891–2898, https://doi.org/10.1021/acsami.6b14469.
[11] D.-H. Park, J.-M. Heo, W. Jeong, Y.H. Yoo, B.J. Park, J.-M. Kim, Smartphone-based VOC sensor using colorimetric polydiacetylenes, ACS Appl. Mater. Interfaces 10 (5) (2018) 5014–5021, https://doi.org/10.1021/acsami.7b18121.
[12] Y. Ishijima, H. Imai, Y. Oaki, Tunable mechano-responsive color-change properties of organic layered material by intercalation, Chem 3 (3) (2017) 509–521, https://doi.org/10.1016/j.chempr.2017.05.013.
[13] D. Park, J. Hong, I.S. Park, C.W. Lee, J. Kim, A colorimetric hydrocarbon sensor employing a swelling-induced mechanochromic polydiacetylene, Adv. Funct. Mater. 24 (33) (2014) 5186–5193, https://doi.org/10.1002/adfm.201400779.
[14] L. Hsu, G.L. Cvetanovich, S.I. Stupp, Peptide amphiphile nanofibers with conjugated polydiacetylene backbones in their core, J. Am. Chem. Soc. 130 (12) (2008) 3892–3899, https://doi.org/10.1021/ja076553s.
[15] G. Wegner, Topochemical reactions of monomers with conjugated triple bonds. III. Solid-state reactivity of derivatives of diphenyldiacetylene, J. Polym. Sci. B 9 (2) (1971) 133–144, https://doi.org/10.1002/pol.1971.110090211.
[16] M.P. Hendricks, K. Sato, L.C. Palmer, S.I. Stupp, Supramolecular assembly of peptide amphiphiles, Acc. Chem. Res. 50 (10) (2017) 2440–2448, https://doi.org/10.1021/acs.accounts.7b00297.
[17] S.R. Diegelmann, N. Hartman, N. Markovic, J.D. Tovar, Synthesis and alignment of discrete polydiacetylene-peptide nanostructures, J. Am. Chem. Soc. 134 (4) (2012) 2028–2031, https://doi.org/10.1021/ja211539j.
[18] B.E.I. Ramakers, S.A. Bode, A.R. Killaars, J.C.M. van Hest, D.W.P.M. Löwik, Sensing cell adhesion using polydiacetylene-containing peptide amphiphile fibres, J. Mater. Chem. B 3 (15) (2015) 2954–2961, https://doi.org/10.1039/C4TB02099E.
[19] S.R. Diegelmann, J.D. Tovar, Polydiacetylene-peptide 1D nanomaterials, Macromol. Rapid Commun. 34 (17) (2013) 1343–1350, https://doi.org/10.1002/marc.201300423.
[20] Y. Kuang, Z.-F. Yao, S. Lim, C. Ngo, M.A. Rocha, D.A. Fishman, H.A.M. Ardoña, Biomimetic sequence-templating approach toward a multiscale modulation of chromogenic polymer properties, Macromolecules 56 (12) (2023) 4526–4540, https://doi.org/10.1021/acs.macromol.3c00403.
[21] J. Nuck, K. Sugihara, Mechanism of polydiacetylene blue-to-red transformation induced by antimicrobial peptides, Macromolecules 53 (15) (2020) 6469–6475, https://doi.org/10.1021/acs.macromol.0c00718.
[22] M. Levitt, Conformational preferences of amino acids in globular proteins, Biochemistry 17 (20) (1978) 4277–4285, https://doi.org/10.1021/bi00613a026.
[23] J.S. Nowick, S. Insaf, The propensities of amino acids to form parallel β-sheets, J. Am. Chem. Soc. 119 (45) (1997) 10903–10908, https://doi.org/10.1021/ja972074p.
[24] H. Cui, A.G. Cheetham, E.T. Pashuck, S.I. Stupp, Amino acid sequence in constitutionally isomeric tetrapeptide amphiphiles dictates architecture of one-dimensional nanostructures, J. Am. Chem. Soc. 136 (35) (2014) 12461–12468, https://doi.org/10.1021/ja507051w.
[25] C.A. Kim, J.M. Berg, Thermodynamic β -sheet propensities measured using a zinc-finger host peptide, Nature 362 (6417) (1993) 267–270, https://doi.org/10.1038/362267a0.
[26] S. Lim, D.L.M. Cordova, A.S. Robang, Y. Kuang, K.S. Ogura, A.K. Paravastu, M. Q. Arguilla, H.A.M. Ardoña, Thermochromic behavior of polydiacetylene nanomaterials driven by charged peptide amphiphiles, Biomacromolecules 24 (9) (2023) 4051–4063, https://doi.org/10.1021/acs.biomac.3c00422.
[27] M.M. Safont-Sempere, G. Fernández, F. Würthner, Self-sorting phenomena in complex supramolecular systems, Chem. Rev. 111 (9) (2011) 5784–5814, https://doi.org/10.1021/cr100357h.
[28] L. Adler-Abramovich, P. Marco, Z.A. Arnon, R.C.G. Creasey, T.C.T. Michaels, A. Levin, D.J. Scurr, C.J. Roberts, T.P.J. Knowles, S.J.B. Tendler, E. Gazit, Controlling the physical dimensions of peptide nanotubes by supramolecular polymer coassembly, ACS Nano 10 (8) (2016) 7436–7442, https://doi.org/10.1021/acsnano.6b01587.
[29] H. Yuan, P. Han, Z. Tao, B. Xue, Y. Guo, D. Levy, W. Hu, Y. Wang, Y. Cao, E. Gazit, R. Yang, Peptide coassembly to enhance piezoelectricity for energy harvesting, ACS Appl. Mater. Interfaces 14 (5) (2022) 6538–6546, https://doi.org/10.1021/acsami.1c20146.
[30] M. Zhou, A.M. Smith, A.K. Das, N.W. Hodson, R.F. Collins, R.V. Ulijn, J.E. Gough, Self-assembled peptide-based hydrogels as scaffolds for anchorage-dependent cells, Biomaterials 30 (13) (2009) 2523–2530, https://doi.org/10.1016/j.biomaterials.2009.01.010.
[31] K.M. Wong, A.S. Robang, A.H. Lint, Y. Wang, X. Dong, X. Xiao, D.T. Seroski, R. Liu, Q. Shao, G.A. Hudalla, C.K. Hall, A.K. Paravastu, Engineering β-sheet peptide coassemblies for biomaterial applications, J. Phys. Chem. B 125 (50) (2021) 13599–13609, https://doi.org/10.1021/acs.jpcb.1c04873.
[32] P. Makam, E. Gazit, Minimalistic peptide supramolecular Co-assembly: expanding the conformational space for nanotechnology, Chem. Soc. Rev. 47 (10) (2018) 3406–3420, https://doi.org/10.1039/C7CS00827A.
[33] D.T. Seroski, X. Dong, K.M. Wong, R. Liu, Q. Shao, A.K. Paravastu, C.K. Hall, G. A. Hudalla, Charge guides pathway selection in β-sheet fibrillizing peptide Co-assembly, Commun. Chem. 3 (1) (2020) 172, https://doi.org/10.1038/s42004-020-00414-w.
[34] K. Takegoshi, S. Nakamura, T. Terao, Dipolar-assisted rotational resonance in magic-angle spinning NMR, Chem. Phys. Lett. 344 (5–6) (2001) 631–637, https://doi.org/10.1016/S0009-2614(01)00791-6.
[35] D. Huang, B.C. Hudson, Y. Gao, E.K. Roberts, A.K. Paravastu, Solid-State NMR Structural Characterization of Self-Assembled Peptides with Selective 13C and 15N Isotopic Labels, 2018, pp. 23–68, https://doi.org/10.1007/978-1-4939-7811-3_2.

[36] C.R. Morcombe, K.W. Zilm, Chemical shift referencing in MAS solid state NMR, J. Magn. Reson. 162 (2) (2003) 479–486, https://doi.org/10.1016/S1090-7807(03)00082-X.
[37] A. Pines, M.G. Gibby, J.S. Waugh, Proton-enhanced NMR of dilute spins in solids, J. Chem. Phys. 59 (2) (1973) 569–590, https://doi.org/10.1063/1.1680061.
[38] E.O. Stejskal, J. Schaefer, J.S. Waugh, Magic-angle spinning and polarization transfer in proton-enhanced NMR, J. Magn. Reson. 28 (1) (1977) 105–112, https://doi.org/10.1016/0022-2364(77)90260-8, 1969.
[39] P.R. Romero, N. Kobayashi, J.R. Wedell, K. Baskaran, T. Iwata, M. Yokochi, D. Maziuk, H. Yao, T. Fujiwara, G. Kurusu, E.L. Ulrich, J.C. Hoch, J.L. Markley, BioMagResBank (BMRB) as a Resource for Structural Biology, 2020, pp. 187–218, https://doi.org/10.1007/978-1-0716-0270-6_14.
[40] D.S. Wishart, B.D. Sykes, F.M. Richards, The chemical shift index: a fast and simple method for the assignment of protein secondary structure through NMR spectroscopy, Biochemistry 31 (6) (1992) 1647–1651, https://doi.org/10.1021/bi00121a010.
[41] W. Qiang, W.M. Yau, J.X. Lu, J. Collinge, R. Tycko, Structural variation in amyloid-beta fibrils from alzheimer's disease clinical subtypes, Nature 541 (7636) (2017) 217–221, https://doi.org/10.1038/nature20814.
[42] J.C. Phillips, R. Braun, W. Wang, J. Gumbart, E. Tajkhorshid, E. Villa, C. Chipot, R. D. Skeel, L. Kale, K. Schulten, Scalable molecular dynamics with NAMD, J. Comput. Chem. 26 (16) (2005) 1781–1802, https://doi.org/10.1002/jcc.20289.
[43] M.T. Nelson, W. Humphrey, A. Gursoy, A. Dalke, L.V. Kale, R.D. Skeel, K. Schulten, NAMD: a parallel, object oriented molecular dynamics program, Int. J. Supercomput. Ap 10 (4) (1996) 251–268.
[44] W. Humphrey, A. Dalke, K. Schulten, VMD: visual molecular dynamics, J. Mol. Graph. Model. 14 (1) (1996) 33, https://doi.org/10.1016/0263-7855(96)00018-5.
[45] A.K. Paravastu, R.D. Leapman, W.-M. Yau, R. Tycko, Molecular structural basis for polymorphism in alzheimer's β-amyloid fibrils, Proc. Natl. Acad. Sci. USA 105 (47) (2008) 18349–18354, https://doi.org/10.1073/pnas.0806270105.
[46] M.T. Colvin, R. Silvers, B. Frohm, Y. Su, S. Linse, R.G. Griffin, High resolution structural characterization of Abeta42 amyloid fibrils by magic angle spinning NMR, J. Am. Chem. Soc. 137 (23) (2015) 7509–7518, https://doi.org/10.1021/jacs.5b03997.
[47] S.G. Zech, A.J. Wand, A.E. McDermott, Protein structure determination by high-resolution solid-state NMR spectroscopy: application to microcrystalline ubiquitin, J. Am. Chem. Soc. 127 (24) (2005) 8618–8626, https://doi.org/10.1021/ja0503128.
[48] V. Daebel, S. Chinnathambi, J. Biernat, M. Schwalbe, B. Habenstein, A. Loquet, E. Akoury, K. Tepper, H. Müller, M. Baldus, C. Griesinger, M. Zweckstetter, E. Mandelkow, V. Vijayan, A. Lange, β-Sheet core of tau paired helical filaments revealed by solid-state NMR, J. Am. Chem. Soc. 134 (34) (2012) 13982–13989, https://doi.org/10.1021/ja305470p.
[49] J.J. Helmus, K. Surewicz, W.K. Surewicz, C.P. Jaroniec, Conformational flexibility of Y145Stop human prion protein amyloid fibrils probed by solid-state nuclear magnetic resonance spectroscopy, J. Am. Chem. Soc. 132 (7) (2010) 2393–2403, https://doi.org/10.1021/ja909827v.
[50] G.T. Debelouchina, G.W. Platt, M.J. Bayro, S.E. Radford, R.G. Griffin, Magic angle spinning NMR analysis of $\beta_2$-microglobulin amyloid fibrils in two distinct morphologies, J. Am. Chem. Soc. 132 (30) (2010) 10414–10423, https://doi.org/10.1021/ja102775u.
[51] Q. Shao, K.M. Wong, D.T. Seroski, Y. Wang, R. Liu, A.K. Paravastu, G.A. Hudalla, C. K. Hall, Anatomy of a selectively coassembled β-sheet peptide nanofiber, Proc. Natl. Acad. Sci. U. S. A 117 (9) (2020) 4710–4717, https://doi.org/10.1073/pnas.1912810117.
[52] K.M. Wong, Y. Wang, D.T. Seroski, G.E. Larkin, A.K. Mehta, G.A. Hudalla, C. K. Hall, A.K. Paravastu, Molecular complementarity and structural heterogeneity within Co-assembled peptide β-sheet nanofibers, Nanoscale 12 (7) (2020) 4506–4518, https://doi.org/10.1039/C9NR08725G.
[53] X. Xiao, A.S. Robang, S. Sarma, J.V. Le, M.E. Helmicki, M.J. Lambert, R. Guerrero-Ferreira, J. Arboleda-Echavarria, A.K. Paravastu, C.K. Hall, Sequence patterns and signatures: computational and experimental discovery of amyloid-forming peptides, PNAS Nexus 1 (5) (2022), https://doi.org/10.1093/pnasnexus/pgac263.